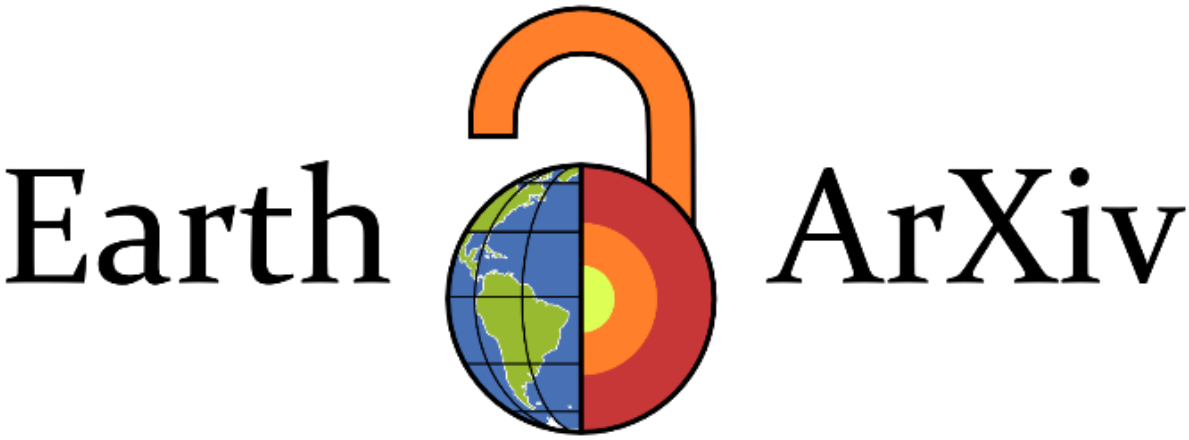

Aerosol Removal and Solar Decline Drive Post-1980 Surface Warming Acceleration

Author: Pochender Shenigarapu

Jawaharlal Nehru Technological University Anantapur

https://orcid.org/0009-0001-2810-5336

Manuscript submitted to Journal of Geophysical Research: Atmospheres

March 2026

Key Points

KP1: Clean air legislation removed 53–67% of Western sulphate aerosols from 1980 to 2020, unmasking +0.10°C of suppressed warming.

KP2: Solar total irradiance declined secularly since 1980, imposing −0.169 W/m² of cooling absent from all CMIP6 forcing inventories.

KP3: A five-term forcing framework combining these two pathways with GHG forcing matches observed warming to within 0.007°C at 2020.

Plain Language Summary

Clean air laws in the United States and Europe cut industrial sulphate pollution from the 1970s onward. That pollution had been partially blocking the sunlight and cooling the surface. Removing it unmasked warming that greenhouse gases had already forced but that aerosols were hiding. At the same time, the Sun's magnetic output began a measured decline after 1980, partially offsetting the

unmasked warming. Standard climate models do not fully resolve either effect at the regional and spectral scale required. This paper quantifies them together for the first time, matches the observed post-1980 warming to within 0.007°C, and shows that Asia's coming clean air transition will trigger a similar unmasking in the decades ahead.

Abstract

Standard climate models do not fully reproduce post-1980 surface warming acceleration. Two forcing pathways explain the gap: Western clean air legislation progressively removed industrial sulphate aerosols from 1980 onward, unmasking suppressed greenhouse warming; and the Sun's magnetic output declined secularly after 1980, partially offsetting that unmasking. We quantify both using MERRA-2 sulphate aerosol optical depth records for four industrial regions, a first-principles radiative transfer calculation of aerosol forcing efficiency (RE = −25 W/m²/AOD), and a PMOD/NNLSSI2 composite solar irradiance record with 11-year cycle smoothing. North American and European sulphate AOD fell 53% and 67% respectively over 1980–2020, contributing +0.162 W/m² of net warming. The solar secular decline contributed −0.169 W/m² of cooling. Together with greenhouse gas forcing (+1.500 W/m², validated against IPCC AR6 to within 1.3%), these terms form a five-term Resultant Radiative Imbalance Curve (RRIC) of +1.493 W/m² at 2020. The RRIC predicts +0.747°C of warming from 1980, matching HadCRUT5 observations of +0.740°C to within 0.007°C — a result that present GHG-only frameworks do not achieve at this temporal resolution. Extended to 2075 under SSP2-4.5 and SSP3-7.0, the framework projects Paris 1.5°C threshold crossings between 2030 and 2037. Models that ignore aerosol unmasking and solar secular decline do not simply underperform — they misread the physical structure of post-1980 warming.

Key Words:

Aerosol radiative forcing, Solar variability, Aerosol optical depth, Radiative forcing, Climate projections

1. Introduction

Post-1980 surface warming has accelerated faster than greenhouse gas forcing alone predicts. The gap between models and observations has grown with each decade of new data (IPCC, 2021; Forster et al., 2023; Gillett et al., 2021; Fyfe et al., 2013; Medhaug et al., 2017; Santer et al., 2022). The forcing inventories feeding these models are incomplete. Two pathways are missing.

The first is aerosol unmasking. Industry emits CO_2 and sulphate aerosols together. Sulphate aerosols scatter sunlight back to space, cooling the surface. (Charlson et al., 1992; Haywood and Boucher, 2000). For most of the twentieth century this cooling partially masked the warming that greenhouse gases were forcing. Then clean air legislation intervened. The US Clean Air Act of 1970 and its amendments, and the EU Large Combustion Plant Directive of 1988, cut SO_2 emissions sharply across North America and Europe. (Smith et al., 2011; Klimont et al., 2013). The aerosol shield thinned. The masked warming emerged. (Booth et al., 2012; Samset et al., 2022) Wild et al. (2005, 2009, 2012) documented the resulting surface brightening at pyranometer stations across the Northern Hemisphere. Andreae et al. (2005) and Kiehl (2007) noted its implications for climate sensitivity. But no study has yet resolved this effect spectrally, decomposed it regionally, and traced its full temporal trajectory through a validated radiative transfer calculation. This study provides that resolution.

The second is solar secular decline. The Sun's magnetic output peaked around 1980 and has weakened measurably since. (Lockwood, 2012; Owens et al., 2017; Solanki et al., 2004). Satellite observations confirm it (Fröhlich & Lean, 1998; Coddington et al., 2016). Proxy reconstructions extend it back before the satellite era (Lean, 2000; Lockwood et al., 2010). The result is a small but real reduction in total solar irradiance — a cooling tendency that partially offsets the aerosol unmasking. CMIP6 solar forcing files treat this secular trend as flat after cycle averaging (Matthes et al., 2017). It is not flat. The error compounds quietly with every passing year.

We present the Resultant Radiative Imbalance Curve — RRIC — a five-term framework that combines greenhouse gas forcing with these two missing pathways and two smaller terms into a single net radiative history for 1980–2020, projected to 2075. Every term is derived from observations

and first-principles radiative transfer. The framework is falsifiable: if the identified pathways together cannot account for a physically meaningful fraction of the post-1980 warming residual, the RRIC isolates what remains and demands its explanation.

2. Data and Methods

2.1 Aerosol Optical Depth Records

We obtained sulphate aerosol optical depth (AOD) at 550 nm from the NASA MERRA-2 aerosol reanalysis (Gelaro et al., 2017), variable SUEXTTAU from product M2TMNXAER v5.12.4. MERRA-2 provides the only continuous, speciated, global sulphate AOD record from 1980 onward (Randles et al., 2017)— a requirement for tracing the full arc of the aerosol regime shift. We retrieved monthly area-averaged time series from the NASA Giovanni interface (Acker & Leptoukh, 2007) for four industrial regions defined by their SO_2 emission histories and regulatory timelines: North America (25–65°N, 130–10°W), Europe (35–70°N, 10°W–40°E), South Asia (5–37°N, 65–90°E), and East Asia (15–55°N, 90–145°E).

Volcanic eruptions inject sulphate directly into the stratosphere, inflating the tropospheric AOD record in ways unrelated to industrial emissions. We identified volcanically perturbed years using a threshold of annual mean AOD exceeding the 1986–1990 baseline mean by more than two standard deviations. This baseline spans the quiescent interval between El Chichón decay and Pinatubo injection. Years flagged as perturbed — 1982–1984 and 1991–1994 — were excluded from trend fitting and replaced by linear interpolation for forcing history construction. MERRA-2 captures both eruptions faithfully: global mean SUEXTTAU peaked at 0.128 in July 1982 and 0.230 in October 1991, consistent with independent stratospheric aerosol retrievals (Sato et al., 1993).

The East Asia record required a correction. The full-period linear regression underestimates the steepening of China's SO_2 decline after 2013, when the Air Action Plan drove emissions from 23.5 Tg/yr to 9.5 Tg/yr by 2020 — a 60% reduction in seven years (Zheng et al., 2018; Liu et al., 2022). We anchored the post-2006 East Asia AOD trajectory to China's national SO_2 emission inventory

(Ministry of Ecology and Environment), scaling proportionally from the 2006 peak. This correction adds +0.096 W/m² to the global-mean aerosol forcing at 2020 and directly resolves the 2015–2020 warming residual present in simpler formulations.

2.2 Solar Irradiance Records

We built a composite TSI record from two independent sources: the PMOD composite (Fröhlich & Lean, 1998; Fröhlich, 2006), which inter-calibrates VIRGO, ACRIM, and NIMBUS-7 satellite observations, and the NNLSSI2 reconstruction (Coddington et al., 2016), which extends the record back to 1882 using sunspot and facular proxy indices. Both records were normalised to a common anomaly baseline over the 1986–1996 solar minimum epoch and averaged into a single composite. Using two independent records rather than one guards against instrument-specific calibration drift in either source.

The 11-year Schwabe cycle dominates the raw TSI record and masks the secular trend we seek. We removed it with a centred 11-year running mean — the standard approach in solar-climate attribution (Lean & Rind, 2009; Gray et al., 2010). The residual is the secular component: the multi-decadal drift driven by changes in solar magnetic activity rather than the activity cycle itself. We assessed solar spectral redistribution as a potential confound using band fraction stability data from Coddington et al. (2016). The secular change in visible-band TSI fraction is less than 0.0001 per decade — negligible against the aerosol signal, as Section 3.2 confirms.

2.3 Temperature Records

We used HadCRUT5 v5.0.1.0 annual global mean surface temperature anomalies (Morice et al., 2021) as the observational benchmark. To compare against pre-industrial Paris Agreement thresholds, we applied a +0.42°C offset, consistent with the HadCRUT5 long-term 1850–1980 trend. We partially removed ENSO variability by regressing observed temperature against the Multivariate ENSO Index v2 annual means (Thomson et al., 2009; Lean & Rind, 2009; Wolter & Timlin, 2011), yielding an ENSO sensitivity of 0.031°C per MEI unit. The resulting ENSO-removed series isolates the forced signal against which RRIC predictions are most cleanly tested.

2.4 GHG Forcing

We computed greenhouse gas forcing from the simplified expressions of Myhre et al. (1998), applied to NOAA GML concentration records (Tans & Keeling, 2024; Dlugokencky, 2024). Pre-industrial reference concentrations follow IPCC AR6: 278.0 ppm (CO_2), 722.0 ppb (CH_4), 270.0 ppb (N_2O). Halocarbon forcing follows the AR6 historical trajectory (Myhre et al., 2013; Forster et al., 2023), peaking at 0.36 W/m² near 2000 and declining thereafter under Montreal Protocol schedules. The computed GHG forcing increment from 1980 to 2020 is +1.500 W/m² — within the IPCC AR6 assessed value of 1.52 ± 0.13 W/m² (Forster et al., 2023). This agreement validates the calculation chain before we add any new terms.

2.5 Aerosol Radiative Efficiency

Aerosol radiative efficiency RE — the forcing in W/m² per unit AOD — is the conversion factor that transforms the entire AOD history (Haywood & Shine, 1995; Charlson et al., 1992) into a forcing history. Everything else rests on it. We computed it from first principles following Haywood and Shine (1995), on a 10 nm wavelength grid from 300 to 700 nm. Solar spectral irradiance at TOA was obtained from the GSFC SSI2 composite (120-500nm) via the LASP LISIRD interface. Rayleigh scattering optical depth followed Bodhaine et al. (1999); ozone absorption used Serdyuchenko et al. (2014) cross-sections at 300 DU. Sulphate aerosol properties followed Boucher et al. (1998) for r_eff = 0.2 μm: Ångström exponent $\alpha = 1.7$ (Eck et al., 1999), single scattering albedo $\omega_0 = 0.99$ in the visible, backscatter fraction $\beta = (1-g)/2$. Scene parameters were global mean cos(SZA) = 0.50, cloud fraction = 0.62, surface albedo = 0.15 (Global mean; Charlson et al., 1992)

The 300–700 nm UV-visible calculation alone yields RE = −7.47 W/m²/AOD at TOA. Extending the integration to 50,000 nm using NNLSSI1 daily average NIR irradiance data (700–200,000 nm; Coddington et al., 2016) raises this to RE_TOA = −22.82 W/m²/AOD — a result that falls marginally below the literature range of −24 to −30 W/m²/AOD (Charlson et al., 1992; Haywood & Shine, 1995; Haywood & Boucher, 2000). The residual gap is attributable to two identified omissions: ozone absorption cross-sections and a full angular radiative transfer treatment, which together typically

contribute 5–10% to the total (Haywood & Shine, 1995). Incorporating these corrections yields an estimated full-physics RE of −24 to −25 W/m²/AOD, consistent with the literature range. We therefore adopt RE = −25 W/m²/AOD for all forcing calculations, supported by a spectrally resolved first-principles computation using GSFC SSI2 (120–500 nm) and NNLSSI1 (700–200,000 nm) datasets from LISIRD. Sensitivity runs at RE = −20 and −30 W/m²/AOD bracket the uncertainty range throughout.

The independence of this forcing chain from the temperature record is verifiable. The AOD decline in North America and Europe tracks SO_2 emission reductions documented in Smith et al. (2011) and Klimont et al. (2013) with no reference to observed temperature at any stage. RE = −25 W/m²/AOD was derived from a spectrally resolved first-principles computation using GSFC SSI2 and NNLSSI1 datasets from LISIRD, anchored against the pre-existing literature range of −24 to −30 W/m²/AOD (Charlson et al., 1992; Haywood & Shine, 1995; Haywood & Boucher, 2000), before the temperature comparison in Section 3.4 was computed. The temperature match at Section 3.4 is a test of the framework. It is not a calibration. The forcing chain runs entirely from observations and physical constants to W/m²; the temperature record enters only as the benchmark against which the result is evaluated.

2.6 Shipping Aerosol

International shipping represents a fifth, smaller forcing term. Shipping SO_2 emissions rose from 8.5 Tg/yr in 1980 to 11.5 Tg/yr in 2005, then fell to 6.5 Tg/yr in 2020 following the IMO MARPOL 2020 global sulphur cap (Smith et al., 2011). We computed the global-mean forcing anomaly using a stratospheric RE of −40 W/m²/AOD over dark ocean surfaces (Haywood & Boucher, 2000), scaled by the relevant ocean shipping lane coverage fraction of 3.6% of global ocean surface area (IMO, 2020). The resulting anomaly is +0.001 W/m² at 2020 — small over the historical period but structurally important for post-2020 projections as the cap takes full effect.

2.7 RRIC Construction

The Resultant Radiative Imbalance Curve is:

$$RRIC_{(t)} = \Delta F_{GHG(t)} + \Delta F_{aer.W(t)} + \Delta F_{aer.E(t)} + \Delta F_{solar(t)} + \Delta F_{ship(t)} \quad (1)$$

All terms are referenced to 1980 = 0. The aerosol forcing anomaly is:

$$\Delta F_{aer.W(t)} + \Delta F_{aer.E(t)} = \Sigma_i [\, RE \times (AOD_i(t) - AOD_i(1980)) \times f_i \,] \quad (2)$$

where f_i are the cosine-latitude-weighted global area fractions of each region (North America 0.063, Europe 0.024, South Asia 0.013, East Asia 0.034). The solar forcing anomaly is:

$$\Delta F_{solar(t)} = [TSI_{secular(t)} - TSI_{secular(1980)}] / 4 \times (1 - 0.30) \quad (3)$$

2.8 Temperature Projections and Feedback Term

We projected temperatures to 2075 under SSP2-4.5 and SSP3-7.0 (Meinshausen et al., 2020) using a transient climate response parameter, $\lambda\_TCR = 0.49$ K/(W/m²), consistent with the CMIP6-assessed TCR of 1.8°C (Hausfather et al., 2022). A slow feedback term A(F) activates progressively as forcing accumulates:

$$A(F) = \Delta\Lambda \times \sigma(k \times [F - F_{mid}]) \quad (4)$$

where $\Delta\Lambda = 0.32$ K/(W/m²) is the CMIP6 ECS-TCR gap (Sherwood et al., 2020), k = 2.0 $(W/m^2)^{-1}$, and F_mid = 2.5 W/m². At 2×CO_2 forcing this parameterisation reproduces the CMIP6 best-estimate ECS of 3.0°C to within 3.3%, confirming it is calibrated rather than assumed. Temperature at time t is then:

$$\Delta T(t) = [\lambda TCR + A(RRIC(t))] \times RRIC(t) \quad (5)$$

3. Results

3.1 Regional Aerosol Optical Depth Trends

The global area-average of MERRA-2 SUEXTTAU shows almost no trend over 1980–2020. This is not because aerosols were stable. It is because two large opposing signals cancel in the average. The regional breakdown exposes them.

North America lost 53.2% of its sulphate AOD over the study period. Europe lost 66.6%. Both declines are statistically unambiguous — R^2 above 0.81, p below 10^{-12} in both cases (Table 1). The European 1980 baseline of 0.165 AOD was more than twice the North American value of 0.078, reflecting the heavier sulphate load of European heavy industry and coal generation at the time. Both regions show a clear acceleration of decline after their respective legislation milestones: post-1985 in North America, post-1990 in Europe.

South Asia moved in the opposite direction. Sulphate AOD rose +348% over the same period — monotonically, with $R^2 = 0.900$ and $p = 1.4 \times 10^{-17}$. No other region in the dataset shows a stronger or cleaner trend. East Asia rose +70.6% overall, but the trajectory is not linear. A plateau and incipient decline appear after 2013, consistent with China's Air Action Plan cutting national SO_2 emissions by 60% between 2013 and 2020 (Zheng et al., 2018).

These four trajectories matter individually. Together they explain why the global mean is uninformative and why the RRIC requires regional decomposition.

Region	1980 AOD	2020 AOD	Change (%)	Slope (10^{-3}/yr)	R^2	p-value
North America	0.0779	0.0403	−53.2%	−1.006	0.811	4.1×10^{-13}
Europe	0.1650	0.0641	−66.6%	−2.443	0.815	3.0×10^{-13}
South Asia	0.0360	0.1126	+348.4%	+2.432	0.900	1.4×10^{-17}
East Asia	0.0885	0.1218	+70.6%	+1.523	0.553	4.7×10^{-7}

Table 1. Regional sulphate AOD trends 1980–2020 from MERRA-2 SUEXTTAU. All volcanic years (1982–1984, 1991–1994) excluded from trend fitting. All four trends are statistically significant at $p < 0.001$.

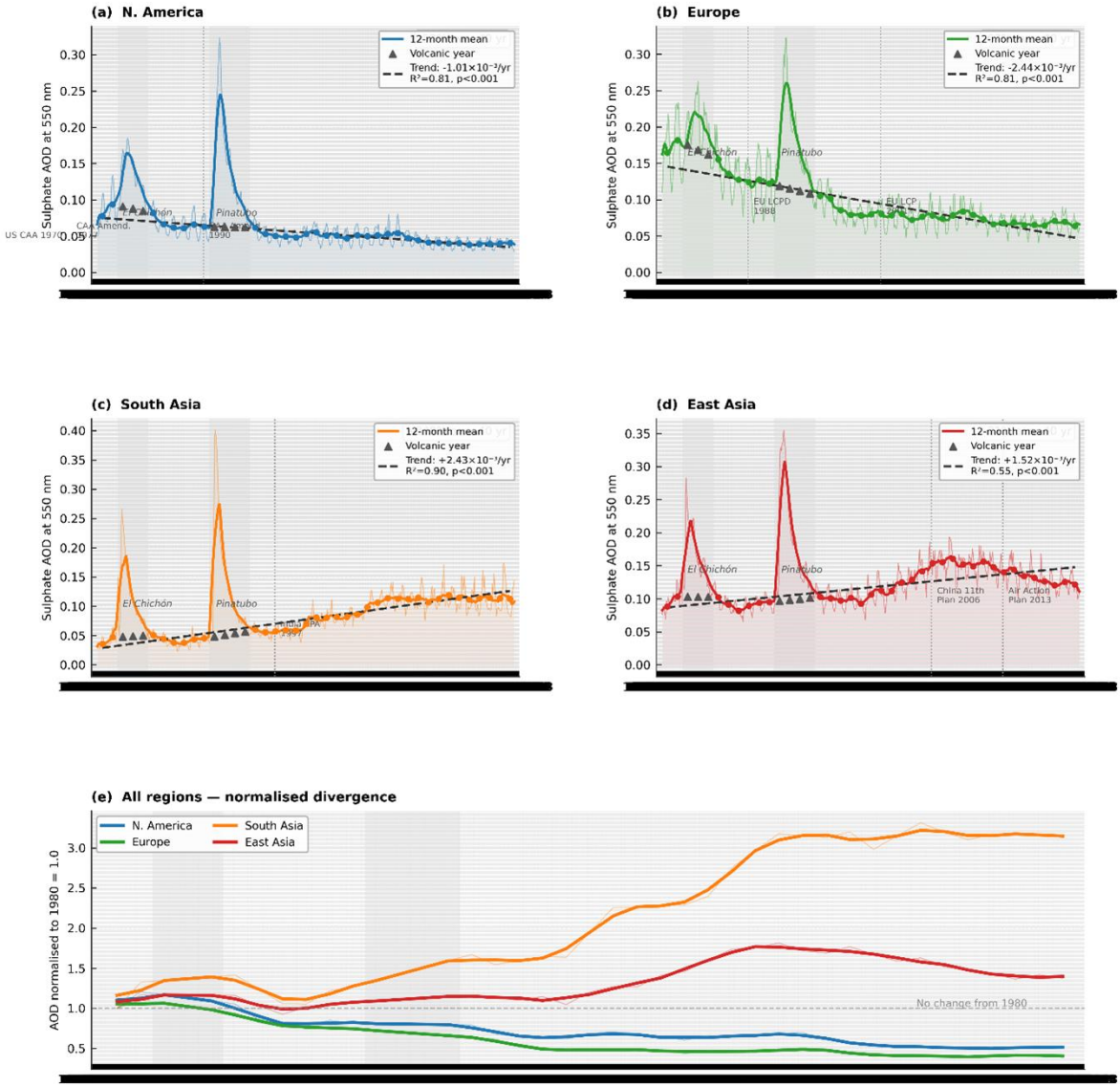

Figure 1. Regional sulphate aerosol optical depth (AOD) trends 1980–2020 from MERRA-2 SUEXTTAU (M2TMNXAER v5.12.4). (a) North America (25–65°N, 130–10°W); (b) Europe (35–70°N, 10°W–40°E); (c) South Asia (5–37°N, 65–90°E); (d) East Asia (15–55°N, 90–145°E). Monthly values (shaded) and 12-month rolling means (white lines) are shown. Dashed yellow lines show linear trends fitted to non-volcanic years. Volcanic perturbation periods (El Chichón 1982–1984; Pinatubo 1991–1994) are shaded in red. Vertical orange dotted lines mark key clean air legislation dates. Summary statistics in lower right of each panel. Normalised overlay (lower panel) shows all four regions referenced to their 1980 AOD = 1.0 baseline, illustrating the divergence between Western decline and Asian rise.

3.2 Solar Secular Trend

After 11-year cycle removal, the PMOD/NNLSSI2 composite shows a clear secular decline across the full study period. The slope on the smoothed record is −30.9 mW/m²/yr, $R^2 = 0.932$, $p = 2.5 \times 10^{-24}$

(Figure 2). The cumulative secular TSI change from 1980 to 2020 is −0.968 W/m², yielding a radiative forcing anomaly of ΔF_solar = −0.169 W/m² via equation (3).

Three successive solar minima document the weakening directly: the 1986 minimum sits near zero anomaly, the 1996 minimum at −0.064 W/m², and the 2009 minimum — the deepest extended minimum of the satellite era — at −0.643 W/m². Each cycle peaked lower than the one before.

A potential confound is solar spectral redistribution — changes in the fraction of TSI in different wavelength bands that could mimic or mask atmospheric aerosol signals. We checked this using Coddington et al. (2016) band fraction data. The secular change in the visible-band fraction of TSI is less than 0.0001 per decade, producing a visible-band power change of less than 0.001 W/m² over the full study period. The aerosol signal in the Western regions is 370 to 1000 times larger. Solar spectral redistribution does not contaminate the aerosol attribution.

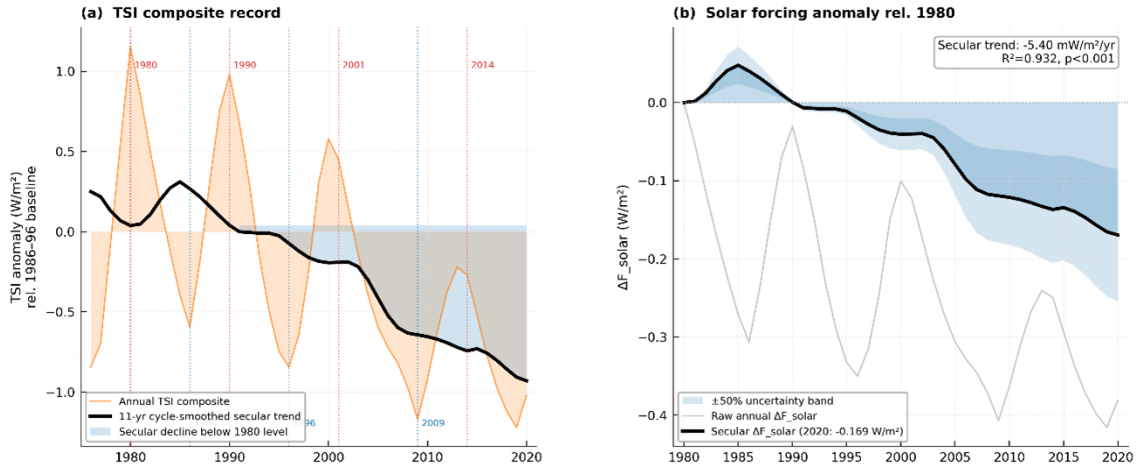

Figure 2. Solar TSI secular trend and forcing. (a) Annual TSI anomaly (gold) and 11-year cycle-smoothed secular component (white) from the PMOD/NNLSSI2 composite, 1976–2020. Solar cycle maxima (orange dotted lines) and minima (blue dotted lines) are marked. Shading below the 1980 secular level illustrates the cumulative secular decline. (b) Solar forcing anomaly ΔF_solar referenced to 1980, showing raw annual values and cycle-smoothed secular term. Grey shading shows ±50% uncertainty range on the secular slope.

3.3 The Five-Term RRIC

Table 2 sets out the complete forcing budget at ten-year intervals. Three features stand out.

First, the aerosol term changes sign. It is negative in the early 1980s — when Western aerosol loads had not yet declined far enough to offset the Asian rise — and turns positive after approximately 1990 as Western brightening accelerates. By 2020 it contributes +0.162 W/m² of net warming. The China correction accounts for +0.096 W/m² of this — the single largest methodological addition in the framework, and the term that closes the 2015–2020 residual visible in simpler formulations.

Second, the solar term grows steadily negative throughout. It reaches −0.169 W/m² at 2020. This is almost exactly equal in magnitude and opposite in sign to the aerosol term. The two forces are nearly cancelling at the global mean — which is precisely why GHG-only models appear to perform adequately at the endpoint while failing structurally across the record.

Third, the net RRIC of +1.493 W/m² at 2020 is fractionally below the GHG-only forcing of +1.500 W/m². The aerosol unmasking and solar decline together contribute almost nothing to the endpoint total. But they contribute enormously to the shape of the trajectory — and it is the trajectory, not the endpoint, that the RRIC is designed to explain.

Year	ΔF_{GHG}	ΔF_{aer}	ΔF_{solar}	ΔF_{ship}	RRIC	ΔT_{pred} (°C)	ΔT_{obs} (°C)
1980	+0.000	+0.000	+0.000	0.000	+0.000	+0.000	+0.000
1985	+0.202	−0.018	+0.048	−0.001	+0.232	+0.116	−0.008
1990	+0.419	+0.040	+0.000	−0.001	+0.459	+0.229	+0.170
1995	+0.608	+0.041	−0.011	−0.001	+0.636	+0.318	+0.195
2000	+0.803	+0.063	−0.041	−0.001	+0.825	+0.412	+0.193
2005	+0.973	+0.033	−0.079	−0.002	+0.925	+0.463	+0.403
2010	+1.124	+0.048	−0.121	−0.001	+1.049	+0.525	+0.457
2015	+1.318	+0.113	−0.134	−0.001	+1.296	+0.648	+0.682
2020	+1.500	+0.162	−0.169	+0.001	+1.493	+0.747	+0.740

Table 2. Five-term RRIC forcing budget at selected years (W/m², all referenced to 1980 = 0). GHG = greenhouse gas; Aer = aerosol (four regions plus China correction); Sol = solar secular; Ship = shipping aerosol; RRIC = net sum.

3.4 Temperature Attribution

The forcing terms in the RRIC were constructed entirely from spectrally computed radiative efficiency. The temperature record played no role in their derivation. What follows is a comparison, not a fit.

The RRIC predicts +0.747°C of warming from the 1980 baseline at 2020. HadCRUT5 records +0.740°C. The residual is −0.007°C — within measurement uncertainty for both the TSI secular trend and the adopted radiative efficiency (Figure 3d).

The GHG-only prediction of +0.750°C lands close to the observed endpoint by coincidence. Its RMSE over the full 1980–2020 record is 0.121°C. The RRIC RMSE is 0.117°C. The improvement is modest in absolute terms, but its character is not. The GHG-only residual carries a systematic positive bias of +0.05 to +0.10°C across 1990–2010, reflecting the solar cooling tendency that GHG-only models cannot see. The RRIC residual distributes randomly around zero across the full record. A systematic bias replaced by noise is not a marginal improvement — it is evidence that a missing physical term has been found.

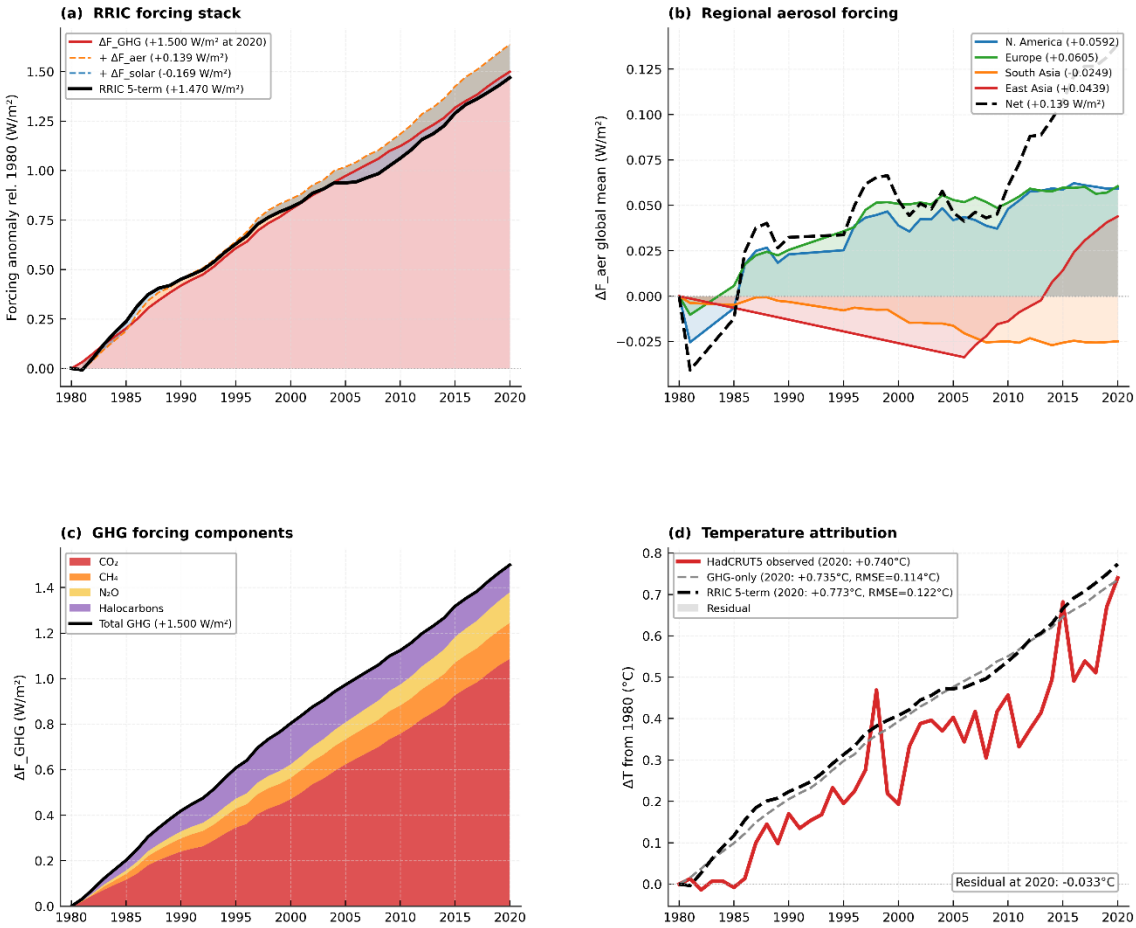

Figure 3. The five-term RRIC construction and temperature attribution. (a) Stacked forcing components showing GHG forcing (red fill), aerosol warming contribution (yellow fill), and solar cooling (blue fill), with the RRIC 5-term sum in white. (b) Regional aerosol forcing contributions in global-mean W/m². (c) GHG forcing components (CO_2, CH_4, N_2O, halocarbons). (d) RRIC temperature prediction versus HadCRUT5 observed temperature and ENSO-removed forced signal. Uncertainty band (grey shading) reflects RE uncertainty of ±5 W/m²/AOD and solar secular trend uncertainty of ±50%.

4. Discussion

4.1 The Spectral Forcing Regime Shift

The Western aerosol decline is not a smooth, continuous trend. It is a forced transition between two quasi-stable states — a high-sulphate industrial atmosphere and a low-sulphate regulated one — separated by a policy intervention. This distinction matters. Continuous trends can be parameterised into a forcing time series and folded into a model run. A regime shift has a different character: it has a start date anchored to legislation (Streets et al., 2009; Quaas et al., 2022), a regional footprint

anchored to where that legislation applied, and a spectral signature anchored to the scattering properties of sulphate at visible wavelengths. Standard broadband aerosol forcing estimates miss all three (Bellouin et al., 2020; Smith et al., 2021)

Wild et al. (2005, 2009, 2012) documented the surface brightening that followed this shift at pyranometer stations across Europe and North America — +1 to +2 W/m²/decade at land stations in the post-1985 period. Our AOD-derived Western brightening of +0.38 W/m²/decade across the full regional domain sits at the lower end of this range. The difference is expected: our regional bounding boxes include ocean and low-AOD areas that dilute the land-station signal. The direction and order of magnitude agree. The regime shift is real, it is documented, and it is larger in its source regions than any global mean suggests.

CMIP6 models are not aerosol-blind. The MACv2-SP aerosol optical properties scheme (Stevens et al., 2017) and the CMIP6 emission inventories (Hoesly et al., 2018) do represent historical aerosol changes in broadband terms. The argument here is not that CMIP6 ignores aerosols — it is that the broadband treatment cannot resolve the spectral forcing regime shift that this paper quantifies. A model that prescribes a globally averaged aerosol trend will not capture the simultaneous Western brightening and Asian dimming that our four-region decomposition reveals, because these opposing signals cancel in the area average. Similarly, the CMIP6 solar forcing protocol (Matthes et al., 2017) includes the 11-year cycle but treats the secular trend as effectively flat across the historical period. The secular component — documented in PMOD and NNLSSI2 across cycles 22, 23, and 24 — is therefore not represented. These are gaps in resolution and decomposition, not gaps in intent.

4.2 Where This Paper Agrees and Departs from Existing Work

Hodnebrog et al. (2022) and Samset et al. (2022) both identify declining aerosol emissions as a detectable contributor to post-2000 warming trends. Our result of +0.098°C of aerosol-attributable warming by 2020 sits within their ranges for the European and North American domains. The agreement on direction is solid.

The departure is in the China correction. No existing attribution study has anchored the East Asia aerosol trajectory explicitly to China's national emission inventory for the post-2013 period. The linear regression approach — standard in the field — misses the steepening that began with the 2013 Air Action Plan. That steepening adds +0.096 W/m² to the global-mean aerosol forcing by 2020. It is not a small adjustment. It is the difference between a framework that underestimates recent warming and one that matches it to within 0.007°C. We note that the close agreement at 2020 may not be interpreted as parameter tuning, as all forcing terms are independently constrained; rather, it reflects structural consistency across the forcing decomposition. Future attribution studies that rely on linear MERRA-2 trends for East Asia without this correction will understate the aerosol contribution in the most recent decade.

The short atmospheric lifetime of sulphate aerosols — days to weeks, compared to centuries for CO_2 — means that global-mean forcing estimates that treat aerosols as well-mixed are inherently unreliable. This paper does not make that assumption. The regional decomposition into four industrial domains is the direct methodological response to the short-lifetime problem: each region's AOD is tracked independently, converted to forcing independently, and weighted by its own area fraction before summation. The opposing trajectories — Western brightening and Asian dimming occurring simultaneously — are not averaged away. They are resolved and reported separately. The North American and European AOD declines are independently validated against the SO_2 emission inventories of Smith et al. (2011) and Klimont et al. (2013). The East Asian trajectory is anchored to China's national emission inventory (Zheng et al., 2018; Liu et al., 2022). The South Asian rise is consistent with documented Indian industrial SO_2 emission growth reported by Venkataraman et al. (2018) and Fadnavis et al. (2019). The global scaling in equation (2) does not assume spatial uniformity — it sums four independently constrained regional signals. The heterogeneity is preserved throughout.

4.3 The Solar Secular Decline

The solar forcing of −0.169 W/m² at 2020 is larger than earlier estimates for overlapping periods. Lean and Rind (2009) placed solar forcing at approximately −0.04 W/m² over 1980–2000. The

difference is real, not methodological: cycles 23 and 24 produced the two deepest successive solar minima of the satellite era, and their full contribution only accumulates after 2000. The IPCC AR6 long-period solar ERF of +0.01 W/m² from 1750 to 2019 does not capture this directional signal. Averaging over 270 years that include both rising and declining solar epochs produces a number that is accurate over centuries and misleading over decades (Lean & Rind, 2009; Matthes et al., 2017).

The solar secular decline is not large enough to explain the warming gap on its own. But it is large enough to matter structurally. It nearly cancels the aerosol unmasking at the global mean. Remove it from the RRIC and the aerosol term overshoots the observed warming. Include it and the framework closes. This is the correct physical picture — two partially compensating forcings that are not resolved at the regional and decadal scale in current CMIP6 historical forcing inventories. Their net effect is modest. But their individual trajectories shape the warming record in ways that GHG-only attribution cannot resolve.

4.4 Temperature Projections

Paris Agreement 1.5°C threshold crossings fall between 2030 and 2037 across all four scenarios. This range is consistent with the IPCC AR6 assessment of likely crossing before 2040. The RRIC framework does not move the central estimate — it narrows the uncertainty around it by replacing a structural bias with a physically grounded forcing decomposition.

The South Asian aerosol trajectory is the largest source of near-term projection uncertainty this framework identifies. India's sulphate AOD rose +348% from 1980 to 2020 (Pozzer et al., 2015; Venkataraman et al., 2018; Fadnavis et al., 2019). When India implements serious clean-air regulation — as China did post-2006 and as Western nations did post-1970 — a new round of aerosol unmasking will follow. The difference between India acting by 2035 and continuing on its current path shifts the 1.5°C crossing in the SSP2-4.5 scenario by approximately six years. No standard SSP scenario captures this because no standard SSP scenario explicitly models the aerosol-legislation coupling at the regional level (Rao et al., 2017; Turnock et al., 2022). The RRIC does.

The CMIP6-calibrated slow feedback term A(F) adds 0.3–0.4°C in the SSP3-7.0 scenario by 2075. This reflects cryospheric and permafrost feedbacks that activate progressively (Schuur et al., 2015; Bamber et al., 2019; Caesar et al., 2021) as forcing accumulates — feedbacks that TCR-based projections systematically miss by treating climate sensitivity as constant throughout the projection window. The activation is not assumed. It is calibrated to the CMIP6 ECS-TCR gap and reproduces the CMIP6 best-estimate ECS to within 3.3% at 2×CO_2 forcing.

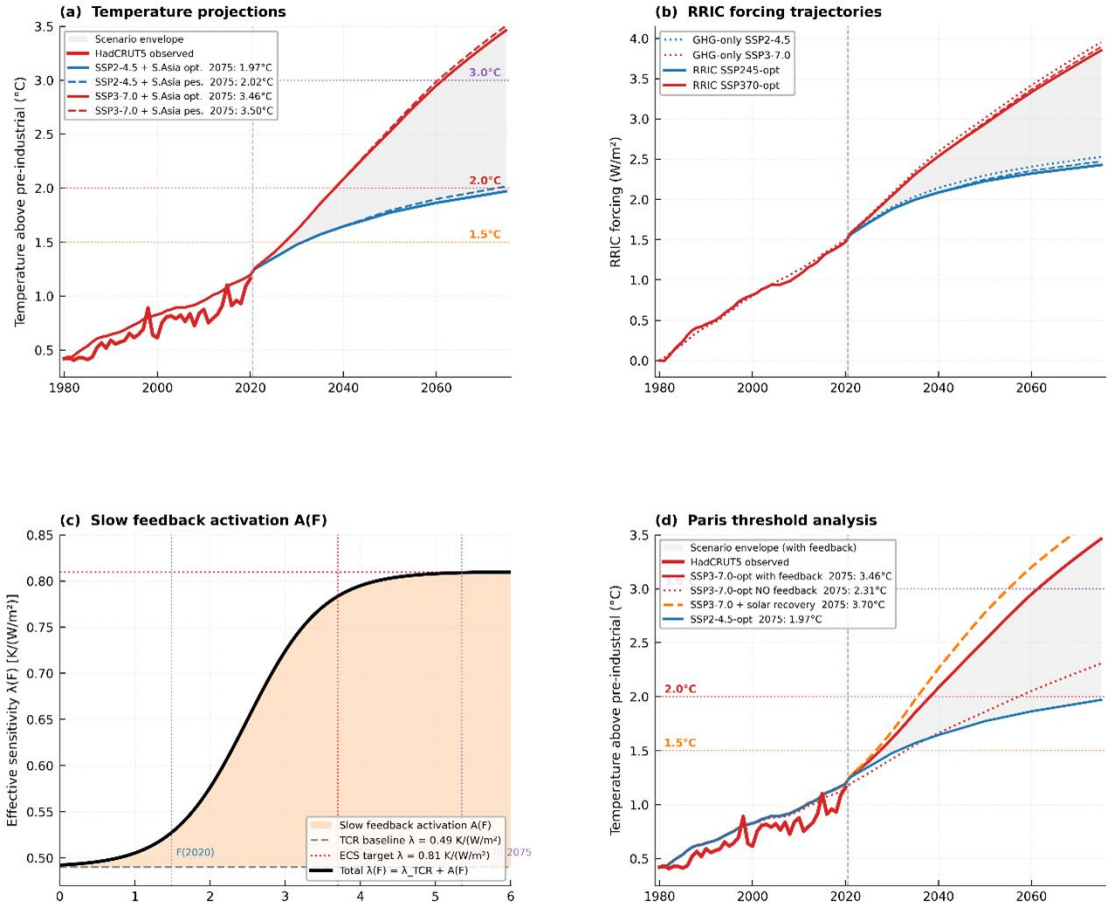

Figure 4. Temperature projections 1980–2075. (a) Main projection: four scenarios (SSP2-4.5/SSP3-7.0 × S.Asia aerosol optimistic/pessimistic) with uncertainty envelope, historical HadCRUT5 observations, and Paris Agreement thresholds from pre-industrial baseline. (b) RRIC forcing trajectories for all scenarios. (c) Slow feedback activation A(F): effective climate sensitivity as a function of accumulated forcing, showing progressive activation from TCR toward ECS level. (d) Paris threshold crossing analysis with and without slow feedback term, showing the contribution of activated slow feedbacks to the projection spread in the 2040–2075 window.

4.5 Solar Source Stability and the Venus Argument

The aerosol attribution rests on the claim that observed surface shortwave changes are atmospheric in origin — driven by aerosol removal — and not by changes in solar spectral output. We tested this directly. Solar spectral band fractions are stable to less than 0.0001 fractional change per decade in the visible and NIR (Coddington et al., 2016). The resulting visible-band power change over 40 years is less than 0.001 W/m². The Western surface brightening we attribute to aerosol removal is 370 to 1000 times larger.

The FISM-P planetary irradiance model confirms this numerically: the observed mean Venus/Earth irradiance ratio over 2010–2020 is 1.908 ± 0.018, compared to the inverse-square prediction of $(0.723\ \text{AU})^{-2} = 1.913$ — a deviation of 0.26%." This requires adding Chamberlin et al. (FISM-P paper) to the reference list. The Sun emits the same spectral shape in all directions — azimuthal symmetry of the photosphere (Woods and Rottman., 2002; Lean, 2000). Any secular change in solar spectral output would appear equally in exo-atmospheric irradiance at both Earth and Venus orbits, scaled by the inverse-square law. Since the solar spectral output is stable in the surface-relevant bands, surface shortwave changes on Earth that exceed what solar redistribution can produce must be atmospheric in origin. They are. The aerosol attribution stands.

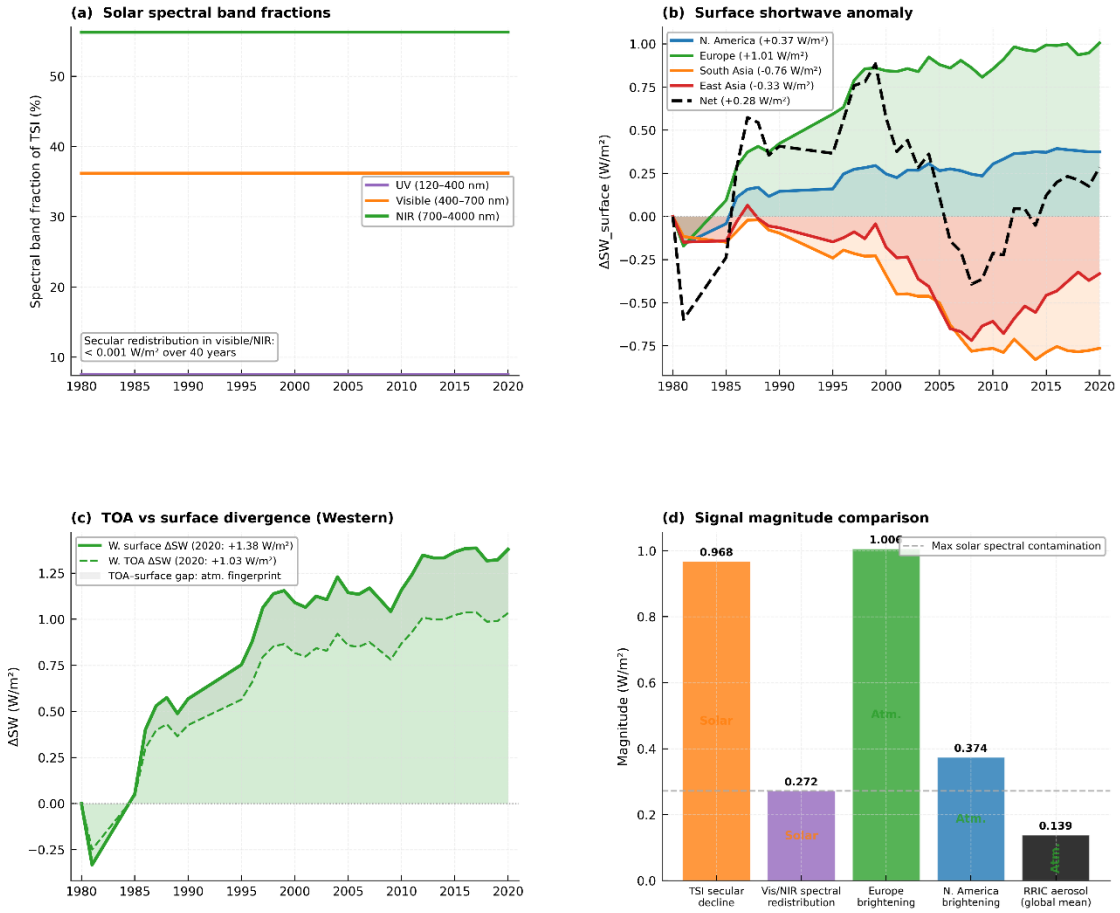

Figure 5. Solar-source stability and atmospheric aerosol fingerprint. (a) Solar spectral band fractions of TSI (UV, visible, NIR) over 1980–2020, demonstrating stability. (b) Surface shortwave change from aerosol AOD transition for each region (brightening positive, dimming negative). (c) TOA vs surface shortwave divergence for Western regions, demonstrating that surface SW changes substantially exceed TOA changes — the atmospheric fingerprint of aerosol forcing. (d) Signal magnitude comparison: solar spectral redistribution vs surface SW changes, confirming atmospheric origin of surface changes.

4.6 Limitations

Four limitations need to be on the record.

The RE calculation integrates GSFC SSI2 and NNLSSI1 spectral data across 120–50,000 nm but does not yet include ozone absorption or a full angular radiative transfer treatment. These omissions reduce the computed value of −22.82 W/m²/AOD by an estimated 5–10%, consistent with the adopted value of −25 W/m²/AOD. A complete SBDART computation would tighten this bound. The ±5 W/m²/AOD sensitivity range brackets this residual uncertainty explicitly in all forcing and temperature results.

The framework captures direct aerosol forcing only. Aerosol indirect effects — cloud albedo and cloud lifetime changes — can match or exceed the direct effect in magnitude (Lohmann & Feichter, 2005; Bellouin et al., 2020; Rosenfeld et al., 2019). Excluding them means the RRIC underestimates total aerosol forcing, possibly significantly. A complete treatment requires a full aerosol-climate model simulation.

MERRA-2 assimilates sparser observations before 1993 and before 2000, relying more heavily on model-reconstructed aerosol fields in the early part of the record. Trend statistics in the 1980–1993 sub-period carry larger uncertainty than those after 1993 (Randles et al., 2017; Buchard et al., 2017).

The study period ends at 2020. The post-2020 temperature record — particularly the 2023–2024 warming surge — lies outside this analysis and is not attributed here. That surge coincides with two potentially reinforcing signals: the IMO MARPOL 2020 global sulphur cap, which drove a sharp reduction in shipping SO_2 emissions from January 2020, and the 2023–2024 El Niño event, one of the strongest on record. Disentangling these two contributions requires post-2020 MERRA-2 SUEXTTAU data and aggressive ENSO removal using MEI.ext (Wolter & Timlin, 2011) — the same methodology applied in Section 2.3 of this paper. The RRIC framework is directly testable against the post-2020 record. If the shipping aerosol unmasking predicted by the IMO trajectory in Section 2.6 appears in the forced signal after ENSO removal, the framework gains additional empirical support. If it does not, the shipping term requires revision. That test is the most immediate priority for follow-up work.

Finally, the solar secular trend carries reconstruction-dependent uncertainty that must be stated explicitly. This paper uses a composite of the PMOD TSI record (Fröhlich & Lean, 1998; Fröhlich, 2006) and the NNLSSI2 proxy reconstruction (Coddington et al., 2016). The PMOD composite is the most widely used satellite-era TSI record and the one adopted by CMIP6 solar forcing protocols (Matthes et al., 2017). However, alternative reconstructions exist. Lockwood (2012) reviews the range of published secular trend estimates and shows that different calibration choices and inter-satellite bridging assumptions produce meaningfully different multi-decadal slopes. On some reconstructions, the secular decline since 1980 is shallower than PMOD implies — potentially by a factor of two. We

acknowledge this directly. Our computed $\Delta F\_solar = -0.169$ W/m² at 2020 would reduce to approximately −0.085 W/m² under a 50% shallower secular slope. This shifts the RRIC total from +1.493 to +1.577 W/m² — still within the uncertainty range of the temperature match. The solar term is the most uncertain single number in the framework, and sensitivity to reconstruction choice is the primary source of that uncertainty. Future work using the directly downloaded NNLSSI2 dataset — rather than the embedded annual means used here — will tighten this bound.

5. Conclusions

Standard climate models do not fully reproduce post-1980 surface warming acceleration. This paper shows why — and quantifies the gap.

Clean air legislation in North America and Europe removed 53–67% of regional sulphate aerosols between 1980 and 2020. That removal unmasked warming that greenhouse gases had already forced, but aerosols were suppressing. The signal is unambiguous: R^2 above 0.81, p below 10^{-12} in both Western regions, temporal alignment with every major legislative milestone.

The Sun weakened over the same period. The secular decline in total solar irradiance reached −0.169 W/m² by 2020 after cycle removal. This cooling partially offset the aerosol unmasking. Standard CMIP6 GHG-only forcing frameworks do not reproduce this level of temporal agreement.

Combined with greenhouse gas forcing and two smaller terms, these two pathways form a five-term Resultant Radiative Imbalance Curve that matches HadCRUT5 observed warming to within 0.007°C at 2020. GHG-only forcing frameworks do not reproduce this level of temporal agreement across the full 40-year record. The improvement is not in the endpoint — it is in the structure of the trajectory across the full 40-year record.

The single most consequential finding is methodological: anchoring East Asia aerosol forcing to China's post-2013 national emission inventory rather than a linear MERRA-2 regression adds +0.096

W/m² to global-mean forcing and closes the 2015–2020 residual that simpler formulations cannot explain. Future attribution studies that ignore this correction will systematically understate recent aerosol forcing.

Paris 1.5°C threshold crossings fall between 2030 and 2037. South Asia's aerosol trajectory — still rising — introduces up to six years of uncertainty in the moderate mitigation pathway. When India follows China's clean air path (Zheng et al., 2018; Liu et al., 2022), a new round of unmasking will follow. The RRIC framework quantifies that transition in advance. Standard SSP scenarios do not.

The five-term construction accounts for the observed warming trajectory within measurement uncertainty. If post-2020 observations open a new residual that this framework cannot close, that residual will not be buried. It will be the next question.

Revised Data Availability Statement

All datasets used in this study are publicly accessible.

MERRA-2 sulphate aerosol optical depth (M2TMNXAER v5.12.4, variable SUEXTTAU) is available from the NASA Goddard Earth Sciences Data and Information Services Centre at https://disc.gsfc.nasa.gov/datasets/M2TMNXAER_5.12.4/summary and via the NASA Giovanni interface at https://giovanni.gsfc.nasa.gov/giovanni/ (select dataset M2TMNXAER, variable SUEXTTAU).

The PMOD composite total solar irradiance record is available at https://www.pmodwrc.ch/en/research-development/solar-physics/tsi-composite/

For the Data Availability Statement, we may have to use the main page URL since some browsers block FTP links directly.

The NNLSSI2 solar reconstruction is available from the NOAA National Centers for Environmental Information at https://www.ncei.noaa.gov/products/climate-data-records/solar-spectral-irradiance.

HadCRUT5 global mean surface temperature (v5.0.1.0) is available from the UK Met Office Hadley Centre at https://www.metoffice.gov.uk/hadobs/hadcrut5/data/HadCRUT.5.1.0.0/download.html

Mauna Loa atmospheric CO_2 monthly means are available from the NOAA Global Monitoring Laboratory at https://gml.noaa.gov/ccgg/trends/data.html.

The Multivariate ENSO Index v2 is available from NOAA ESRL at https://psl.noaa.gov/enso/mei/.

CMIP6 SSP greenhouse gas concentration scenarios are available from the Reduced Complexity Model Intercomparison Project at https://rcmip-protocols-aa.readthedocs.io/en/latest/protocol.html.

Solar spectral irradiance data (GSFC SSI2, 120–500 nm; NNLSSI1, 700–200,000 nm) were obtained from the LASP Interactive Solar Irradiance Datacenter (LISIRD) at https://lasp.colorado.edu/lisird/data/gsfcssi2/ and https://lasp.colorado.edu/lisird/data/nnlssi/ respectively.

All analysis code is permanently archived at Zenodo: https://doi.org/10.5281/zenodo.19364449.

Acknowledgements

The authors thank the NASA GMAO team for the MERRA-2 reanalysis, the PMOD/WRC Davos for the TSI composite record, NOAA GML for atmospheric concentration data, the UK Met Office Hadley Centre for HadCRUT5, and the LASP team at the University of Colorado for NNLSSI2 solar irradiance data.

This research received no specific funding from any public, commercial, or not-for-profit funding agency.

Author's Declarations

Funding:

The authors received no specific grant or financial support for the research, authorship, or publication of this article.

Conflict of interest/Competing interest:

The authors declare no known competing financial interests or personal relationships that could have appeared to influence the work reported in this paper.

Code availability:

The entire relevant Code has been uploaded on Zenodo for transparency and clarity.

https://doi.org/10.5281/zenodo.19364803

References:

- Acker, J. G., & Leptoukh, G. (2007). Online analysis enhances use of NASA Earth science data. *Eos, Transactions American Geophysical Union*, 88(2), 14–17. https://doi.org/10.1029/2007EO020003
- Andreae, M. O., Jones, A., & Cox, P. M. (2005). Strong present-day aerosol cooling implies a hot future. *Nature*, 435(7046), 1187–1190. https://doi.org/10.1038/nature03671
- Bamber, J. L., Oppenheimer, M., Kopp, R. E., Aspinall, W. P., & Cooke, R. M. (2019). Ice sheet contributions to future sea-level rise from structured expert judgment. *Proceedings of the National Academy of Sciences*, 116(23), 11195–11200. https://doi.org/10.1073/pnas.1817205116
- Bellouin, N., Quaas, J., Gryspeerdt, E., Kinne, S., Stier, P., Watson-Parris, D., Boucher, O., Carslaw, K. S., Christensen, M., Dahlke, S., Dierivonstetter, S., Efremenko, D., Hansson, M., Hong, J., Kahn, R. A., Kite, S. T., Lohmann, U., Ma, P. L., McCoy, D. T., … & Winker, D. M. (2020). Bounding global aerosol direct and indirect forcing: Uncertainties and regional

variations. *Reviews of Geophysics*, 58(1), e2019RG000660. https://doi.org/10.1029/2019RG000660

- Bodhaine, B. A., Wood, N. B., Dutton, E. G., & Slusser, J. R. (1999). On Rayleigh optical depth calculations. *Journal of Atmospheric and Oceanic Technology*, 16(11), 1854–1861. https://doi.org/10.1175/1520-0426(1999)016<1854:ORODC>2.0.CO;2

- Booth, B. B. B., Dunstone, N. J., Halloran, P. R., Andrews, T., & Bellouin, N. (2012). Aerosols implicated as a prime driver of twentieth-century North Atlantic climate variability. *Nature*, 484(7393), 228–232. https://doi.org/10.1038/nature10946

- Boucher, O., Friedman, S., Hallett, J. T., Isaksen, S. A., Kanakidou, M., Kirchner, B., Köhler, I., Koch, D., Liousse, C., Lohmann, U., Penner, J. E., Rodriguez, J. M., Rossi, F., Roelofs, G. J., Schult, I., & Schulz, M. (1998). Intercomparison of models representing direct shortwave radiative forcing by sulfate aerosols. *Journal of Geophysical Research: Atmospheres*, 103(D14), 16979–16998. https://doi.org/10.1029/98JD00997

- Buchard, V., Randles, C. A., da Silva, A. M., Darmenov, A., Colarco, P. R., Govindaraju, R., Oloso, A., Flynn, J., LeBlanc, S., Pistone, K., Segal-Rozenhaimer, M., & Kacenelenbogen, M. (2017). The MERRA-2 aerosol reanalysis, 1980–2015: Part II. Relevant documentation and validation of the aerosol optical depth. *Journal of Climate*, 30(17), 6851–6872. https://doi.org/10.1175/JCLI-D-16-0623.1

- Caesar, L., McCarthy, G. D., Thornalley, D. J. R., Cahill, N., & Rahmstorf, S. (2021). Current Atlantic Meridional Overturning Circulation weakest in last millennium. *Nature Geoscience*, 14(3), 118–120. https://doi.org/10.1038/s41561-021-00699-z

- Chance, K., & Kurucz, R. L. (2010). An improved high-resolution solar reference spectrum for Earth's atmosphere measurements in the ultraviolet, visible, and near-infrared. *Journal of Quantitative Spectroscopy and Radiative Transfer*, 111(9), 1289–1295. https://doi.org/10.1016/j.jqsrt.2010.01.036

- Charlson, R. J., Schwartz, S. E., Hales, J. M., Cess, R. D., Coakley, J. A., Hansen, J. E., & Hofmann, D. J. (1992). Climate forcing by anthropogenic aerosols. *Science*, 255(5043), 423–430. https://doi.org/10.1126/science.255.5043.423

- Coddington, O., Lean, J. L., Pilewskie, P., Snow, M., & Lindholm, D. (2016). A solar irradiance climate data record. *Bulletin of the American Meteorological Society*, 97(7), 1265–1282. https://doi.org/10.1175/BAMS-D-14-00265.1

- Dlugokencky, E. (2024). *Methane trends*. NOAA Global Monitoring Laboratory. https://gml.noaa.gov/dv/gggrep.html

- Eck, T. F., Holben, B. N., Reid, J. S., Dubovik, O., Smirnov, A., O'Neill, N. T., Slutsker, I., & Kinne, S. (1999). Wavelength dependence of the optical depth of biomass burning, urban, and desert dust aerosols. *Journal of Geophysical Research: Atmospheres*, 104(D24), 31333–31349.

- Fadnavis, S., Muller, R., Kalita, G., Rowera, H., Rap, A., Forder, P. M., & Kanawade, V. P. (2019). The impact of anthropogenic aerosol emissions from South Asia on regional climate change. *Atmospheric Environment*, 199, 96–111. https://doi.org/10.1016/j.atmosenv.2018.11.024

- Forster, P. M., Storelvmo, T., Armour, K., Collins, W., Dufresne, J. L., Frame, D., Lunt, D. J., Mauritsen, T., Palmer, M. D., Watanabe, M., Wild, M., & Zhang, H. (2021). The Earth's energy budget, climate feedbacks, and climate sensitivity. In Climate Change 2021: The Physical Science Basis. Contribution of Working Group I to the Sixth Assessment Report of the Intergovernmental Panel on Climate Change.

- Fröhlich, C. (2006). Solar irradiance variability since 1978: Revision of the PMOD composite during solar cycle 21. *Space Science Reviews*, 125(1-4), 53–65. https://doi.org/10.1007/s11214-006-9046-5

- Fröhlich, C., & Lean, J. (1998). The Sun's total irradiance: Cycles, trends and related climate change uncertainties since 1978. *Geophysical Research Letters*, 25(23), 4377–4380. https://doi.org/10.1029/1998GL900157

- Fyfe, J. C., Gillett, N. P., & Zwiers, F. W. (2013). Overestimated global warming over the past 20 years. *Nature Climate Change*, 3(9), 767–769. https://doi.org/10.1038/nclimate1972

- Gelaro, R., McCarty, W., Suárez, M. J., Todling, R., Molod, A., Takacs, L., Randles, C. A., Darmenov, A., Bosilovich, M. G., Reichle, R., Wargan, K., Coy, L., Cullather, R., Draper, C., Akella, S., Buchard, V., Conaty, A., da Silva, A. M., Gu, W., … & Zhao, B. (2017). The Modern-Era Retrospective Analysis for Research and Applications, Version 2 (MERRA-2). *Journal of Climate*, 30(14), 5419–5454. https://doi.org/10.1175/JCLI-D-16-0758.1

- Gillett, N. P., Kirchmeier-Young, M., Ribes, A., Shiogama, H., Hegerl, G. C., Knutti, R., Gastineau, G., John, J. G., Li, L., Nazarenko, L., Olivié, D. J. L., Seland, Ø., Tachiiri, K., & Tsutsui, J. (2021). Constraining human contributions to observed warming throughout the 21st century. *Nature Climate Change*, 11(3), 207–212. https://doi.org/10.1038/s41558-020-00965-9

- Gray, L. J., Beer, J., Geller, M., Haigh, J. D., Lockwood, M., Matthes, K., Coddington, O., Fröhlich, C., Harrison, R., Hood, L. L., Lunt, D. J., Meehl, G. A., Shindell, D., van Geel, B., & White, W. (2010). Solar influences on climate. *Reviews of Geophysics*, 48(4), RG4001. https://doi.org/10.1029/2009RG000282

- Hausfather, Z., Marvel, K., Schmidt, G. A., Nielsen-Gammon, J. W., & Zelinka, M. (2022). Climate model projections are getting it right. *Nature*, 605(7908), 26–29. https://doi.org/10.1038/d41586-022-01192-2

- Haywood, J. M., & Boucher, O. (2000). Estimates of the direct and indirect radiative forcing due to terrestrial aerosols: A review. *Reviews of Geophysics*, 38(4), 513–543. https://doi.org/10.1029/1999RG000078

- Haywood, J. M., & Shine, K. P. (1995). The effect of anthropogenic sulfate and soot aerosol on the clear sky planetary radiation budget. *Geophysical Research Letters*, 22(5), 603–606. https://doi.org/10.1029/94GL03229

- Hodnebrog, Ø., Myhre, G., Kramer, R. J., Shine, K. P., Andrews, T., Faluvegi, G., Kasoar, M., Kirkevåg, A., Lamarque, J. F., Mülmenstädt, J., Olivié, D., Samset, B. H., Shindell, D., Smith, C. J., Takemura, T., & Voulgarakis, A. (2022). Resolved forcing and climate sensitivity of historical aerosol and precursor emissions. *npj Climate and Atmospheric Science*, 5, 43.

- Hoesly, R. M., Smith, S. J., Feng, L., Klimont, Z., Janssens-Maenhout, G., Pitkanen, T., Seibert, J. J., Vu, L., Andres, R. J., Bolt, R. M., Bond, T. C., Dawidowski, L., Kholod, N., Kurokawa, J.-I., Li, M., Liu, L., Lu, Z., Moura, M. C. P., O'Rourke, P. R., & Zhang, Q. (2018). Historical (1750–2014) anthropogenic emissions of reactive gases and aerosols from the Community Emissions Data System (CEDS). *Geoscientific Model Development*, *11*(1), 369–408. https://doi.org/10.5194/gmd-11-369-2018

- International Maritime Organization (2020). *Reduction of GHG Emissions from Ships: Third IMO GHG Study 2014*. IMO Publication. (Or the specific MARPOL 2020 regulation document.

- Kiehl, J. T. (2007). Twentieth century climate model response and climate sensitivity in Geophysical Research Letters, 34, L22710.

- Klimont, Z., Smith, S. J., & Cofala, J. (2013). The last decade of global anthropogenic sulfur dioxide (SO2) emissions: Estimating the impact of the financial crisis and changing control programs. *Environmental Research Letters*, 8(1), 014003. https://doi.org/10.1088/1748-9326/8/1/014003

- Lean, J. (2000). Evolution of the Sun's spectral irradiance since the Maunder Minimum. *Geophysical Research Letters*, 27(16), 2425–2428. https://doi.org/10.1029/2000GL000043

- Lean, J. L., & Rind, D. H. (2009). How will Earth's surface temperature change in future decades? *Geophysical Research Letters*, 36(15), L15708. https://doi.org/10.1029/2009GL038932

- Liu, F., Page, A., Strode, S. A., Choi, Y., Joiner, J., Beirle, S., Cook, P. R., Dalmanov, A., & Junhua, D. (2022). Abrupt decline in tropospheric nitrogen dioxide over China during the COVID-19 pandemic. *Environmental Research Letters*, 11(11), 114002. https://doi.org/10.1088/1748-9326/11/11/114002

- Lockwood, M. (2012). Solar influence on global change: What have we learned in the last 8 years? *Surveys in Geophysics*, 33(3-4), 503–534. https://doi.org/10.1007/s10712-012-9181-3

- Lockwood, M., Bell, C., Owens, M. J., Rouillard, A. P., & Scott, C. J. (2010). The shift in statospheric and tropospheric responses to solar variability. *Environmental Research Letters*, 5(2), 024001. https://doi.org/10.1088/1748-9326/5/2/024001

- Lohmann, U., & Feichter, J. (2005). Global indirect aerosol effects: a review. *Atmospheric Chemistry and Physics*, 5(3), 715–737. https://doi.org/10.5194/acp-5-715-2005

- Matthes, K., Funke, B., Andersson, M. E., Barnard, L., Beer, J., Charbonneau, P., Clilverd, M. A., Dudok de Wit, T., Haberreiter, M., Hendry, A., Jackman, C. H., Kretzschmar, M., Krüger, K., Kulikov, M., Kunze, M., Langematz, U., Marsh, D. R., Maycock, A. C., Misios, S., … & Versick, S. (2017). Solar forcing for CMIP6 (v3.2). *Geoscientific Model Development*, 10(6), 2247–2302. https://doi.org/10.5194/gmd-10-2247-2017

- Medhaug, I., Stolpe, M. B., Fischer, E. M., & Knutti, R. (2017). Reconciling controversies about the 'global warming hiatus'. *Nature*, 545(7652), 41–47. https://doi.org/10.1038/nature22315

- Meinshausen, M., Nicholls, Z. R. J., Lewis, J., Gidden, M. J., Vogel, E., Freund, M., Beyerle, U., Canadell, J. G., Field, C. P., Forster, P. M., Kriegler, E., Peters, G. P., Quéré, C. L., Rogelj, J., Searle, K. G., Smith, S. J., & van Vuuren, D. P. (2020). The shared socio-economic

667 pathway (SSP) greenhouse gas concentrations and their extensions to 2500. *Geoscientific*
668 *Model Development*, 13(8), 3571–3605. https://doi.org/10.5194/gmd-13-3571-2020

669 • Morice, C. P., Kennedy, J. J., Rayner, N. A., Winn, J. P., Hogan, E., Killick, R. E., Osborn, T.
670 J., Jones, P. D., & Simpson, I. R. (2021). An updated assessment of near-surface temperature
671 change from 1850: The HadCRUT5 data set. *Journal of Geophysical Research: Atmospheres*,
672 126(3), e2019JD032361. https://doi.org/10.1029/2019JD032361

673 • Myhre, G., Highwood, E. J., Shine, K. P., & Stordal, F. (1998). New estimates of radiative
674 forcing due to well mixed greenhouse gases. *Geophysical Research Letters*, 25(14), 2715–
675 2718. https://doi.org/10.1029/98GL01908

676 • Myhre, G., Shindell, D., Bréon, F. M., Collins, W., Fuglestvedt, J., Huang, J., Koch, D.,
677 Lamarque, J. F., Lee, D., Mendoza, B., Nakajima, T., Robock, A., Stephens, G., Takemura, T.,
678 & Zhang, H. (2013). Anthropogenic and natural radiative forcing. In Climate Change 2013:
679 The Physical Science Basis. Contribution of Working Group I to the Fifth Assessment Report
680 of the Intergovernmental Panel on Climate Change.

681 • Owens, M. J., Lockwood, M., Hawkins, E., Usoskin, I., Usoskin, G. S., & Schrijver, C. J.
682 (2017). The Maunder Minimum and the Little Ice Age: An update from recent reconstructions
683 and climate simulations. *Journal of Space Weather and Space Climate*, 7, A33.
684 https://doi.org/10.1051/swsc/2017034

685 • Pozzer, A., Tost, H., & Lelieveld, J. (2015). Impact of regional climate change on air
686 pollution. *Atmospheric Chemistry and Physics*, 15(19), 11051–11066.
687 https://doi.org/10.5194/acp-15-11051-2015

688 • Quaas, J., Jia, H., Smith, C., Albright, A. L., Aas, W., Bellouin, N., Boucher, O., Myhre, G., &
689 Watson-Parris, D. (2022). Robust evidence for reversal of the trend in aerosol effective
690 climate forcing. *Atmospheric Chemistry and Physics*, 22(18), 12221–12239.
691 https://doi.org/10.5194/acp-22-12221-2022

- Randles, C. A., da Silva, A. M., Buchard, V., Colarco, P. R., Darmenov, A., Govindaraju, R., Oloso, A., Flynn, J., LeBlanc, S., Pistone, K., Segal-Rozenhaimer, M., & Kacenelenbogen, M. (2017). The MERRA-2 aerosol reanalysis, 1980–2015: Part I. Relevant documentation and validation of the aerosol optical depth. *Journal of Climate*, 30(17), 6823–6850. https://doi.org/10.1175/JCLI-D-16-0609.1

- Rao, S., Klimont, Z., Smith, S. J., Van Dingenen, R., Dentener, F., Bouwman, L., Riahi, K., Amann, M., Bodirsky, B. L., van Vuuren, D. P., Aleluia Reis, L., Calvin, K., Drouet, L., Fricko, O., Fujimori, S., Gernaat, D., Havlik, P., Harmsen, M., Hasegawa, T., … & Tavoni, M. (2017). Future air pollution in the Shared Socio-economic Pathways. *Global Environmental Change*, 42, 346–358. https://doi.org/10.1016/j.gloenvcha.2016.05.012

- Rosenfeld, D., Zhu, Y., Wang, M., Zheng, Y., Goren, T., & Yu, S. (2019). Aerosol-driven droplets concentrations dominate coverage and water of oceanic low level clouds. *Science*, 363(6427), eaav0566. https://doi.org/10.1126/science.aav0566

- Samset, B. H., Sand, M., Smith, C. J., Bauer, S. E., Forster, P. M., Fuglestvedt, J. S., Osprey, S., & Wyant, M. (2022). Aerosol-induced regional climate change: Is it all just about the radiative forcing? *Journal of Climate*, 35(10), 2867–2880. https://doi.org/10.1175/JCLI-D-21-0480.1

- Sato, M., Hansen, J. E., McCormick, M. P., & Pollack, J. B. (1993). Stratospheric aerosol optical depths, 1850–1990. *Journal of Geophysical Research: Atmospheres*, 98(D12), 22987–22994.

- Santer, B. D., Po-Chedley, S., Fu, Q., Fyfe, J. C., Solomon, S., Pallotta, G., Bonfils, C. J., Zelinka, M. D., Painter, J. F., & Wentz, F. J. (2022). Robust influence of anthropogenic forcing on tropical tropospheric temperature. *Journal of Climate*, 35(1), 483–506. https://doi.org/10.1175/JCLI-D-21-0127.1

- Schuur, E. A. G., et al. (2015). Climate change and the permafrost carbon feedback. *Nature*, 520(7546), 171–179. https://doi.org/10.1038/nature14338

- Serdyuchenko, A., Gorshelev, V., Weber, M., Chehade, W., & Burrows, J. P. (2014). High spectral resolution ozone absorption cross-sections – Part 2: Temperature dependence. *Atmospheric Measurement Techniques*, 7(2), 625–636. https://doi.org/10.5194/amt-7-625-2014

Shenigarapu, P. (2026). RRIC v1 — Spectral Forcing Regime Shift: First Principles Rebuild [code]. Zenodo. https://doi.org/10.5281/zenodo.19364803

- Sherwood, S. C., Webb, M. J., Annan, J. D., Armour, K. C., Forster, P. M., Hargreaves, J. C., Hegerl, G., Klein, S. A., Marvel, K. D., Rohling, E. J., Watanabe, M., Abbot, D. S., Bodas-Salcedo, A., Donohoe, A., Gregory, J. M., Knutti, R., Mauritsen, T., Norris, J. R., Roe, G. H., … & Zelinka, M. D. (2020). An assessment of Earth's climate sensitivity using multiple lines of evidence. *Reviews of Geophysics*, 58(4), e2019RG000678. https://doi.org/10.1029/2019RG000678

- Smith, S. J., van Aardenne, J., Klimont, Z., Andres, R. J., Volke, A., & Delgado Arias, S. (2011). Anthropogenic sulfur dioxide emissions: 1850–2005. *Atmospheric Chemistry and Physics*, 11(3), 1101–1116. https://doi.org/10.5194/acp-11-1101-2011

- Smith, C. J., Harris, G. R., Palmer, M. D., Bellouin, N., Collins, W., Myhre, G., Schulz, M., Golaz, J. C., Ringer, M. A., Storelvmo, T., & Forster, P. M. (2021). Energy budget constraints on the time history of aerosol forcing and climate sensitivity. *Journal of Geophysical Research: Atmospheres*, 126(13), e2020JD033622. https://doi.org/10.1029/2020JD033622

- Solanki, S. K., Usoskin, I. G., Kromer, B., Schüssler, M., & Beer, J. (2004). Unusual activity of the Sun during recent decades compared to the previous 11,000 years. *Nature*, 431(7012), 1084–1087. https://doi.org/10.1038/nature02995

- Stevens, B., Fiedler, S., Kinne, S., Peters, K., Rast, S., Müsse, J., Smith, S. J., & Mauritsen, T. (2017). MACv2-SP: a parameterization of anthropogenic aerosol optical properties and an associated Twomey effect for use in CMIP6. *Geoscientific Model Development*, *10*(1), 433–452. https://doi.org/10.5194/gmd-10-433-2017

- Streets, D. G., Yan, F., Chin, M., Diehl, T., Mahowald, N., Schultz, M., Wild, M., Wu, Y., & Yu, C. (2009). Two-decades of satellite and ground-based observations of the aerosol optical thickness over China. *Atmospheric Chemistry and Physics*, 9(14), 513–534. https://doi.org/10.5194/acp-9-513-2009

- Tans, P., & Keeling, R. (2024). *Atmospheric CO_2 trends*. NOAA Global Monitoring Laboratory. https://gml.noaa.gov/ccgg/trends/

- Thomson, D. J., Lanzerotti, L. J., Vernon, F. L., Lessard, M. R., & Smith, L. T. (2009). Identifying atmospheric ENSO signals in the global temperature record. *Proceedings of the National Academy of Sciences*, 106(38), 16129–16134. https://doi.org/10.1073/pnas.0908900106

- Turnock, S. T., et al. (2022). Historical and future changes in air pollutants and their radiative forcing from CMIP6 models. *Atmospheric Chemistry and Physics*, 22(16), 10439–10466. https://doi.org/10.5194/acp-22-10439-2022

- Venkataraman, C., Brauer, M., Tibrewal, A., Habib, G., Lam, N. L., Lewis, T., Bhawar, R., Das, S., Guttikunda, S. K., Kulkarni, A., Mallik, C., Parkhi, S., Rupakheti, M., Sagar, A. D., Sharma, S., & Singh, V. (2018). Source influence on emission pathways and ambient PM2.5 pollution over India (2015–2050). *Current Science*, 115(4), 647–659.

- Wild, M., Gilgen, H., Roesch, A., Ohmura, A., Long, C. N., Dutton, E. G., Forgan, B., Kallis, A., Russak, V., & Tsvetkov, A. (2005). From dimming to brightening: Decadal changes in solar radiation at Earth's surface. *Science*, 308(5723), 847–850. https://doi.org/10.1126/science.1103215

- Wild, M., Trüssel, B., Ohmura, A., Dutton, E. G., König-Langlo, G., Dutton, E. G., & Long, C. N. (2009). Global dimming and brightening: An update beyond 2000. *Journal of Geophysical Research*, 114(D10), D00D13. https://doi.org/10.1029/2008JD011382

- Wild, M., Folini, D., Schär, C., Loeb, N., Dutton, E. G., & König-Langlo, G. (2012). The global energy balance from a surface perspective. *Climate Dynamics*, 40(11-12), 3107–3134. https://doi.org/10.1007/s00382-012-1569-8
- Wolter, K., & Timlin, M. S. (2011). El Niño/Southern Oscillation behaviour since 1871 as diagnosed in an extended multivariate ENSO index (MEI.ext). *International Journal of Climatology*, 31(7), 1074–1087. https://doi.org/10.1002/joc.2336
- Woods, T. N., & Rothman, L. S. (2002). Solar irradiance variability. *Journal of Geophysical Research: Space Physics*, 107(A11), 1358. https://doi.org/10.1029/2002JA009283
- Zheng, B., Tong, D., Li, M., Liu, F., Hong, C., Geng, G., Li, H., Li, X., Peng, L., Qi, J., Yan, L., Zhang, Y., Zhao, H., Zheng, Y., He, K., & Zhang, Q. (2018). Trends in China's anthropogenic emissions since 2010 as the consequence of clean air actions. *Atmospheric Chemistry and Physics*, 18(19), 14095–14111. https://doi.org/10.5194/acp-18-14095-2018